Journal of Statistical Physics, Vol. 77, Nos. 1/2, 1994

Relaxation and Localization in Interacting Quantum Maps

A. Lakshminarayan[1] and N. L. Balazs[2]

Received July 7, 1993; final October 7, 1993

Quantum relaxation is studied in coupled quantum baker's maps. The classical systems are exactly solvable Kolmogorov systems, for which the exponential decay to equilibrium is known. They model the fundamental processes of transport in classically chaotic phase space. The quantum systems, in the absence of global symmetry, show a marked saturation in the level of transport, as the suppression of diffusion in the quantum kicked rotor, and eigenfunction localization in the position basis. In the presence of a global symmetry we study another model that has classically an identical decay to equilibrium, but quantally shows resonant transport, no saturation, and large fluctuations around equilibrium. We generalize the quantization to finite multibaker maps. As a byproduct we introduce some simple models of quantal tunneling between classically chaotic regions of phase space.

KEY WORDS: Relaxation; quantum chaos; baker's map; quantum baker's map; quantum multibaker map.

1. INTRODUCTION

The approach to thermal equilibrium proceeds via a mixing process in phase space engendered by strong global chaos on the energy shell. The presence of such strong chaoticity in low-dimensional deterministic dynamical systems is one of the important discoveries of the modern theory of dynamical systems and has been reviewed extensively (see, for example, Percival[21]). Many features of classical chaos have been explored with the help of classical maps, whether as Poincaré sections of the actual flow in phase space or as abstract transformations of some manifold.

[1] Department of Physics, State University of New York Stony Brook, Stony Brook, New York 11794. E-mail: BALAZS@nuclear.physics.sunysb.edu.

0022-4715/94/1000-0311$07.00/0

The study of quantum systems with a view toward the manifestations of chaoticity has also been extensive.[3,4] The concept of low-dimensional maps plays a central role in the study of classical dynamical systems. This idea can also be exploited to study quantum dynamical systems. Such quantum maps *have* been constructed and provide some of the simplest models to study the quantum manifestations of classical chaos. The quantum maps studied either quantize time-periodic systems[5] or abstract maps like the cat map[6] and baker's map.[7] In these cases we interpret a quantum map as a unitary operator which propagates states during one time step, has the proper classical limit, and preserves classical symmetries. Recently Bogomolny has constructed semiclassical quantum maps from classical Poincaré sections.[8] Quantum maps indeed provide the simplest models to study the quantal manifestations of classical chaos.

In this paper we use quantum maps to investigate the relaxation of a quantum system to equilibrium. One of the deterministic classical systems (a representative of a large class of maps) that we will be quantizing is strongly chaotic and is isomorphic to a stochastic Markov chain. This exactly solvable system consisting of three coupled baker's maps was studied by Elskens and Kapral[1] to model chemical rate laws and to study the microscopic origins of the rate constants. We can think of it as modeling two regions in phase space that are chaotic within each other and that are coupled by a mixing mechanism that can be controlled by a parameter. The rate of relaxation to global equilibrium would depend on this parameter. We will call such a map the three-bakers' map.

Similar situations arise in the study of classical transport, when diffusion is impeded by the presence of partial barriers like cantori.[8] A phase point might be trapped in a given region of phase space for a long time and then ejected to some other region to again spend a long time there. The presence of this trapping could significantly affect quantum transport. Such effects have been studied and reviewed by Bohigas *et al.*[10] using random matrix theory and the model of coupled quartic oscillators. Our present interest in these simple maps is threefold: (a) we wish to introduce an interaction between chaotic maps; (b) we want to investigate how far quantum effects combined with the interaction introduce new time scales or modify old ones; (c) we want to create simple maps which admit tunneling phenomena upon quantization.

The quantization of the bakers' map[7] allows us to quantize the three-bakers' map in a similar fashion. As a byproduct of this quantization we get some simple models of tunneling in quantum systems with chaotic classical limits. We display the eigenangle splitting in one such model.

In Section 2 we introduce and discuss the classical models to be quantized. In Section 3 we quantize these maps as well as quantize two other

finite multibaker maps.[20] In Section 4 we present the numerical results and in Section 5 we discuss these results. We end with a summary in Section 6.

2. THE CLASSICAL MAPS

2.1. The Maps

Since the first map we are quantizing is essentially that introduced by Elskens and Kapral, we refer to their work[1] for a very exhaustive and illuminating discussion of these maps. Here we provide only the essential details necessary to understand the present paper. All the maps below are area-preserving and piecewise linear. The second map is a variant of that studied in ref. 1, and we introduce it due to reasons that will become apparent when we discuss the quantum maps in Section 3.

The phase space is the square $[0, 1) \times [0, 1)$ and is composed of two regions or "cells" $A[0, 1/2) \times [0, 1)$ and $B[1/2, 1) \times [0, 1)$ within which we will place bakers so that there is perfect mixing within regions A and B, but there is no exchange of phase space densities between them. Then we will introduce a third baker in the region or "cell" $C[(1-\alpha)/2, (1+\alpha)/2) \times [0, 1)$. Here $0 \leqslant \alpha \leqslant 1$ is the horizontal width of the overlapping cell C which provides the mixing among the cells A and B; α is the control parameter or the strength of the "interaction", $\alpha/2$ is the overlap of C in each of the disjoint cells A and B. See Fig. 1(c).

The first two maps we will consider below have *identical* classical relaxation behaviors, *but their quantal versions are vastly different* (we will introduce further models in Section 3 that will share some of these relaxation laws). The first map, F_α^1 is essentially identical to the construction in ref. 1, except for the details of scaling and choice of labels p and q. We write F_α^1 as a composition of three baker's maps, M_A, M_B, and M_C. The map M_A acts on region A and it leaves the rest of phase space unaffected. If $(q, p) \in A$ and $M_A(q, p) = (q', p')$, then

$$(q', p') = \begin{cases} (2q, p/2), & 0 \leqslant q < 1/4 \\ (2q - 1/2, (p+1)/2), & 1/4 \leqslant q < 1/2 \end{cases} \tag{1}$$

If $(q, p) \in B$ and $M_B(q, p) = (q', p')$, then

$$(q', p') = \begin{cases} (2q - 1/2, p/2), & 1/2 \leqslant q < 3/4 \\ (2q - 1, (p+1)/2), & 3/4 \leqslant q < 1 \end{cases} \tag{2}$$

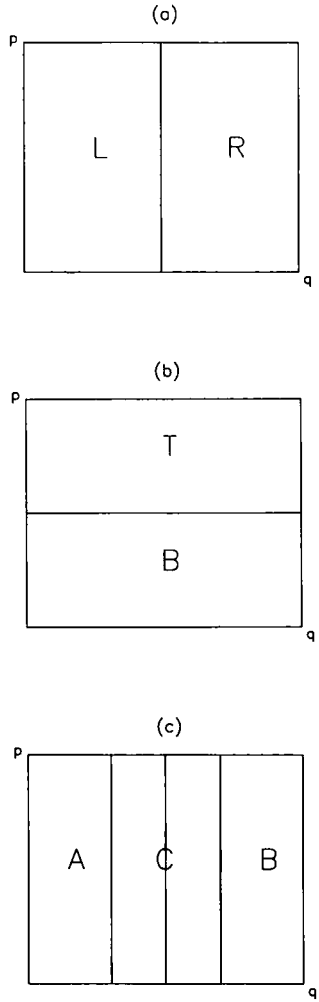

Fig. 1. (a) The baker's map partition before the transform. Left and right partitions are marked. (b) The partition after one time step. L goes into B, and R goes into T. (c) The "cells" A, B, and C shown schematically for the maps $F_{\alpha}^{1,2}$. The width of the rectangle C is α.

If $(q, p) \in C$ and $M_C(q, p) = (q', p')$, then

$$(q', p') = \begin{cases} (2q - (1-\alpha)/2, p/2), & (1-\alpha)/2 \leqslant q < 1/2 \\ (2q - (1-\alpha)/2, (p+1)/2), & 1/2 \leqslant q < (1+\alpha)/2 \end{cases} \tag{3}$$

$$F_\alpha^1 = M_C M_B M_A \tag{4}$$

We also define just the mixing within the cells A and B, without the interaction (two rectangular bakers side by side in cells A and B) as M_{AB}^1,

$$M_{AB}^1 = M_A M_B \tag{5}$$

To distinguish the case when there is an interaction from that when there are only noninteracting disjoint bakers, we have introduced the symbol F. (Here and in the rest of the paper, *superscripts on M, F, and B are indices and not powers.* Any exception to this rule will be explicitly indicated.) Thus the cells A and B have disjoint bakers and the baker in C effects a communication between them. When $\alpha = 0$, there is no interaction. Elskens and Kapral[1] showed that the transformation F_α^1 had strongly ergodic properties. For rational values of α, they constructed finite Markov partitions.[11] They showed that when $\alpha = 1/2$, the transformation F_α^1 is isomorphic to a Bernoulli shift. The motion is ergodic with respect to the usual Lebesgue measure, the area. This implies that the Lyapunov exponent, the measure of the rate of exponential separation of nearby points, is $\lambda = (1+\alpha)$ Log 2. All sufficiently smooth phase space densities evolve into the uniform distribution, a unique equilibrium distribution.

The second map we will study, F_α^2, has identical dynamics in cells A and C; we have bakers defined in them via M_A and M_C [Eqs. (1) and (3)], in cell B we reflect the baker of cell A about the line $q = 1/2$ instead of translating it. The entire dynamics in cells A and B, M_{AB}^2 without the interaction C, is as follows. If $M_{AB}^2(q, p) = (q', p')$,

$$(q', p') = \begin{cases} (2q - 1/2, p/2), & 0 \leqslant q < 1/4 \\ (2q - 1/2, (p+1)/2), & 1/4 \leqslant q < 3/4 \\ (2q - 1, p/2), & 3/4 \leqslant q < 1 \end{cases} \tag{6}$$

The complete transformation, F_α^2, during one time step is

$$F_\alpha^2 = M_C M_{AB}^2 \tag{7}$$

2.2. The Relaxation Laws

The classical steady state is described by the microcanonical ensemble. The approach to this equilibrium is evidently governed by the parameter α;

the larger the value of α, the faster will be the approach to the steady state. The generally expected exponential relaxation to equilibrium is realized in the maps $F_\alpha^{1,2} \equiv F_\alpha$ (We do not write the superscripts when we do not want to distinguish between the two maps.) We can find the relaxation laws by calculating suitable correlation functions. We do not expect there to be qualitative differences for slightly differing values of the parameter α, and we concentrate on $\alpha = 1/2,\ 1/4,\ 1/8$. For these cases we can find the explicit relaxation behaviors via the Markov matrices that describe the Markov processes isomorphic to these maps. Irrational α values do not permit a finite partition, but, as noted in ref. 1, we expect the relaxation to be close to that of the rational approximations of α. We do not unduly bother about this because the very act of quantization imposes the requirement that α be rational. We relegate details of the Markov matrices to Appendix A.

We consider the correlation between two densities given by the characteristic functions χ_A and χ_B defined as follows:

$$\chi_{A,B}(q,p) = \begin{cases} 1, & (q,p) \in A, B \\ 0, & \text{otherwise} \end{cases} \tag{8}$$

We then propagate the density χ_A in time and find its overlap with χ_B. This is the transition rate from region A to B for a density that is initially uniformly distributed in A,

$$F_\alpha^t \chi_A(q,p) = \begin{cases} 1, & F_\alpha^{-t}(q,p) \in A \\ 0, & \text{otherwise} \end{cases} \tag{9}$$

Here t is the time and takes values over the set of integers. The relaxation law is described by the correlation function

$$C_\alpha(t) = \int_0^1 \int_0^1 \chi_B(q,p)\, F_\alpha^t \chi_A(q,p)\, dq\, dp \tag{10}$$

The simplicity of the model of three bakers allows us to evaluate exactly these correlation functions. For $\alpha = 1/2,\ 1/4,\ 1/8$ they are

$$C_{1/2}(t) = (1 - 2^{-t})/4 \tag{11}$$

$$C_{1/4}(t) = (2 - \beta_1 \lambda_1^t - \beta_2 \lambda_2^t)/8 \tag{12}$$

$$C_{1/8}(t) = (4 - \beta_3 \lambda_3^t - \beta_4 \lambda_4^t - \beta_4^* \lambda_4^{*t})/16 \tag{13}$$

The first of these equations is given in ref. 1, and the others can be derived from the respective Markov partitions. (We indicate how to do this in Appendix A; see Fig. 2). The approximate values of the constants are

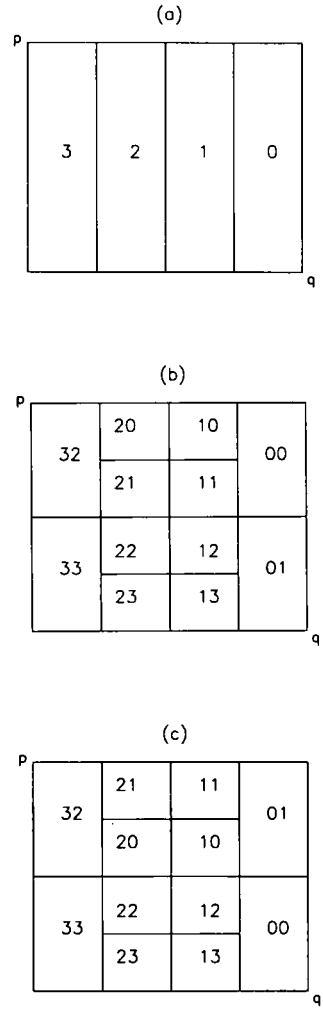

Fig. 2. (a) The partition for the maps $F^{1,2}_{1/2}$. (b) The partition after one time step for the map $F^{1}_{1/2}$. This is the partition into which the partition of (a) has evolved. (c) The partition after one time step for the map $F^{2}_{1/2}$.

$\beta_1 = 1.8944$, $\beta_2 = 2 - \beta_1$, $\lambda_1 = 0.8090$, $\lambda_2 = 1/2 - \lambda_1$, $\beta_3 = 3.8479$, $\beta_4 = 0.07601 + i0.0113$, $\lambda_3 = 0.9196$, $\lambda_4 = -0.2098 + i0.3031$.

We observe that there is an exponential decay or relaxation to the uniform distribution. The relaxation is in general a sum of exponentials with small oscillatory contributions; thus there are multiple relaxation times. The λ_i, $i = 1, 2, 3, 4$, above are not the Lyapunov exponents, and are independent characteristics of the mixing system. During the first time step the slope of the relaxation curves are approximately α, while for a further short linear regime the slope is approximately $\alpha/2$; thereafter the relaxation is exponential.

The Markov partitions of the map F_α^2 may be taken to be the same as that of F_α^1; hence the classical relaxation laws (11)–(13) are *identical*. This of course does not mean that all the details of the classical mechanics are identical (for example, the exact locations of the periodic orbits are different), but the "macroscopic" quantities of the systems, such as entropy, Lyapunov exponents, and correlation functions, are identical. This pair of classical models are interesting, *because different microscopic dynamics generate not only the same equilibrium quantities, but also the same irreversible macroscopic behavior*. Two further models we will be studying are described in Section 3.3. In Section 4 we will be comparing $C_\alpha(t)$ with their quantal equivalents.

2.3 Classical Symmetries

The map F_α^1 has several symmetries that were not discussed in ref. 1, presumably because they have no direct relevance to the classical relaxation mechanisms described above. However, we can anticipate that these not only will significantly modify quantal transport, but most also be preserved for a correct quantization. Consider first the map F_α^1. M_A and M_B, or together M_{AB}^1 inherit the symmetries of the usual bakers' maps defined by them. It is invariant under the following symmetry operations.

1. $R_A: p \to 1 - p$, $q \to 1/2 - q$, for cell A. This is the reflection symmetry about the center of the rectangular cell A.
2. $R_B: p \to 1 - p$, $q \to 3/2 - q$, for cell B. This is the reflection symmetry about the center of the rectangular cell B.
3. $R: p \to 1 - p$, $q \to 1 - q$, for the entire phase space square. This is the global reflection symmetry about the center of the square.
4. $T: q \to (1/2 + q) (\text{mod } 1)$, this is the global symmetry of translation in position by 1/2.

These are all canonical phase space symmetries that must be preserved by the quantization. They are not independent of each other, as a translation by 1/2 followed by a reflection about the center of the square is equivalent to reflection about the individual cells, but it is convenient to define them as here. The quantization proceeds piecewise; we will first quantize the "free" maps $M_{AB}^{1,2}$ and then quantize the interaction. Thus we will require the quantal version of M_{AB}^{1} to preserve all the canonical symmetries listed above. When we add the interaction M_C, the symmetries R_A, R_B, and T break, but due to the reflection symmetry of the interaction the global R symmetry is preserved.

In the case of the map F_α^2, there is the reflection symmetry about the individual cells A and B, R_A and R_B, but there is no global R or T symmetries. Instead there is an anticanonical symmetry S due to spatial reflection about the line $q = 1/2$ ($p \to p$, $q \to 1 - q$). There are many ways in which we can break R and T symmetries, but, as noted earlier, the advantage of F_α^2 is that it shares the same relaxation laws as F_α^1.

In the next section we will write down the quantal propagators corresponding to the classical maps F_α^1 and F_α^2. We will also quantize two finite "multibaker maps."[20] We relegate some details of the quantization to the Appendix *B*.

3. THE QUANTUM MAPS

In this section we will write down the unitary quantal propagators, or quantum maps. The method of quantizing these maps which have no Hamiltonian generating them is facilitated by the quantization procedures of Balazs and Voros[7] developed for the usual baker's map. We note that there is no "canonical" method to construct the propagator, but the quantum baker of ref. 7 has proved to be a natural example and has been studied from several points of views.[12-15] The semiclassical trace can be written as a periodic orbit sum,[13,14] and heavy scaring has been noted in its eigenfunctions.[15] The eigenangle statistics show level repulsion and fall into the universality class of GOE random matrices. There are no eigenangle degeneracies and all eigenangles are irrational multiples of 2π. It is thus a prototype for the study of the quantal manifestations of classical chaos.

3.1. The Propagators

The classical phase space used above is the unit square (using units such that the maximum position and momentum values are unity). One can make the classical phase space compact by identifying the opposite

edges, turning it thereby into a torus, and making the originally finite p and q periodic.

The original phase torus can be divided into N phase cells of size h. Thus, according to the original ideas of Planck, the dynamical system has N states and the state space is an N-dimensional vector space. Since the original momentum and position operators are not periodic operators, we replace them with their unitary extensions, denoted as V and U. The eigenvectors of U are the position eigenkets $|q_n\rangle$ and the eigenvectors of V are the momentum eigenkets $|p_m\rangle$, with $m, n = 0, 1, 2, ..., N-1$. The transformation functions between the eigenstates of position and momentum are given by

$$(G_N)_{nm} \equiv \langle q_n \mid p_m \rangle = \frac{1}{\sqrt{N}} e^{(2\pi i/N)(n+1/2)(m+1/2)} \tag{14}$$

Following Saraceno,[15] we have adopted antiperiodic boundary conditions for the states $|q_n\rangle$ and $|p_m\rangle$. With V the unitary translation operator in position, we have

$$\langle q_{m+1}| = \langle q_m| \, V \tag{15}$$

and

$$\langle q_{m+N}| = -\langle q_m| = \langle q_m| \, V^N \tag{16}$$

This requirement introduces the 1/2 in the phase of the Fourier transforms of Eqn. (14) and facilitates the preservation of classical phase space symmetries. This essentially places the position and momentum eigenvalues at half-integer rather than at integer sites.

The unitary operator corresponding to the classical map M^1_{AB} (just two noninteracting bakers placed side by side in cells A and B) in the position representation is given by

$$B^1_{AB} = G_N^{-1} \begin{pmatrix} G^L_{N/2} & 0 & G^R_{N/2} & 0 \\ 0 & G^L_{N/2} & 0 & G^R_{N/2} \end{pmatrix} \tag{17}$$

Although this looks like a rectangular matrix, it is, in fact, a square one. The matrices $G^L_{N/2}$ and $G^R_{N/2}$ are *rectangular* matrices of dimensions $N/2 \times N/4$. They are simply the vertical left and right halves of the square matrix $G_{N/2}$, i.e.,

$$(G_{N/2})_{mn} = \begin{cases} (G^L_{N/2})_{mn}, & 0 \leqslant m \leqslant N/2-1, \quad 0 \leqslant n \leqslant N/4-1 \\ (G^R_{N/2})_{mn}, & 0 \leqslant m \leqslant N/2-1, \quad N/4 \leqslant n \leqslant N/2-1 \end{cases} \tag{18}$$

while 0 is the null $N/2 \times N/4$ matrix. Thus the "free" propagator B^1_{AB} is a product of two simple matrices, and remarkably enough it is unitary. G_N^{-1} is a unitary matrix, and the unitarity of the second matrix term follows from the unitarity of $G_{N/2}$, for this implies the following;

$$G^L_{N/2} G^{L\dagger}_{N/2} + G^R_{N/2} G^{R\dagger}_{N/2} = I_{N/2}, \tag{19}$$

$$G^{L\dagger}_{N/2} G^L_{N/2} = G^{R\dagger}_{N/2} G^R_{N/2} = I_{N/4} \tag{20}$$

$$G^{L\dagger}_{N/2} G^R_{N/2} = G^{R\dagger}_{N/2} G^L_{N/2} = 0_{N/4} \tag{21}$$

Here $I_{N/4}$ and $I_{N/2}$ are the $N/4 \times N/4$ and $N/2 \times N/2$ identity matrices and $0_{N/4}$ is the $N/4 \times N/4$ null matrix.

The propagator for the map M^2_{AB}, which is a baker in cell A and a reflected baker in cell B, is given by

$$B^2_{AB} = G_N^{-1} \begin{pmatrix} G^L_{N/2} & 0 & 0 & G^R_{N/2} \\ 0 & G^L_{N/2} & G^R_{N/2} & 0 \end{pmatrix} \tag{22}$$

which again is a unitary matrix. Thus we have the "free" propagators $B^{1,2}_{AB}$. A few observations are in order here. These propagators are not in a *block diagonal* form, and thus they engender the quantal phenomenon of *tunneling*. The *classically isolated bakers in cells A and B are not quantally isolated.* This was *forced* upon us because we chose to quantize the phase space as a *whole*. We could have considered the bakers in cells A and B to act on disjoint Hilbert spaces of dimensions $N/2$. This would simply give us in the position representation the propagator

$$B_{\text{sc}} = \begin{pmatrix} B_{N/2} & 0 \\ 0 & B_{N/2} \end{pmatrix} \tag{23}$$

Here $B_{N/2}$ is the baker on $N/2$ states; the baker for N states is given by the matrix of Eq. (B8), Appendix B.

This propagator would neglect quantal tunneling, and we can consider it as a semiclassical propagator. Indeed, while quantizing the interacting baker in cell C we will adopt such a procedure, as we do not know how to do it otherwise. This will not alter qualitatively the relaxation behavior, as we expect such tunneling to be quite small. In Section 3.3 we will introduce models that do not require such piecewise quantization. The remarkable fact is that B_{sc} and B^1_{AB} which we have constructed from purely dynamical arguments must be near in all matrix metrics, and should tend toward each other in the limit of large N. The numerical comparison (not presented here) of relaxation laws engendered by these two class of

matrices supports this statement. A more rigorous comparison of these two families is yet to be done.

Quantizing the action of M_C requires fixing a portion of the state space and "baking" the rest. We will require $N\alpha$ to be an integer, and we take as the interaction the unitary matrix

$$B_C = \begin{pmatrix} I_{(1-\alpha)N/2} & 0 & 0 \\ 0 & B_{N\alpha} & 0 \\ 0 & 0 & I_{(1-\alpha)N/2} \end{pmatrix} \tag{24}$$

Here $B_{N\alpha}$ is the baker transform on $N\alpha$ states, and it provides the interaction between cells A and B. Thus the full propagators quantizing the classical maps F_α^1 and F_α^2, given by Eqs. (4) and (7), are

$$U_\alpha^1 = B_C B_{AB}^1 \tag{25}$$

and

$$U_\alpha^2 = B_C B_{AB}^2 \tag{26}$$

Here the subscript α explicitly shows the parameter dependence, or the strength of the interaction, and has nothing to do with the dimension of the matrices, which is N. The superscripts distinguish between the maps F_α^1 and F_α^2. We recollect that classical relaxation laws for the values of $\alpha = 1/2$, $1/4$, $1/8$ are given by Eqs. (11)–(13).

3.2. Quantum Symmetries

This section verifies that the "free" propagators introduced in the previous section preserve the classical symmetries discussed in Section 2. The implications of these symmetries on the spectrum are discussed. As we shall see, this generates significant differences between the classical and quantal results. The classical map M_{AB}^1, as we recall, is simply two bakers side by side in cells A and B; we take as its quantum map the unitary matrix B_{AB}^1 of Eq. (17). The classical map had the symmetries R_A, R_B, R, and T, which are reflections about the center of the cells A and B, reflection about the center of the square, and translation by 1/2. The quantal operator corresponding to T is simply the unitary translation operator of $N/2$ sites in position ($T_N = V^{N/2}$). This is diagonal in the momentum representation and is given by

$$(T_N)_{mm'} = e^{i\pi(m+1/2)}\delta_{m'm} \tag{27}$$

$T_N^2 = -1$ due to the antiperiodic boundary conditions on the states, and hence the eigenvalues of T_N are $\pm i$.

The operator B^1_{AB}, evaluated explicitly in the *momentum* representation, is given by

$$\langle p_m | B^1_{AB} | p_{m'} \rangle = \frac{\sqrt{2}\, i}{2N} \frac{e^{-i\pi(2m-m'+1/2)/2} - 1}{\sin \pi(2m-m'+1/2)/N} \cdot (1 + e^{-i\pi(m-m')}) \cdot \begin{cases} 1, & 0 \leqslant m \leqslant N/2 - 1 \\ e^{-i\pi(m'-1)/2}, & N/2 \leqslant m \leqslant N-1 \end{cases} \tag{28}$$

Any matrix $A_{mm'}$ commutes with T_N if and only if its entries are nonzero when either both m and m' are even or both are odd. It is easily seen from the factor $(1 + e^{-i\pi(m-m')})$ that this is true for $(B^1_{AB})_{mm'}$. Hence we have

$$[B^1_{AB}, T_N] = 0 \tag{29}$$

(Here we are being sloppy in using the same symbols for the abstract operator and its representation in a particular basis. Of course when computing the commutator we would take the same basis for both operators.) Thus the quantal model has the translation by 1/2 symmetry.

For the other symmetries, it would be easier to write the operators in the position basis. We introduce two functions

$$\frac{1}{\nu(m,n)} = \sin(\pi(m-2n-1/2)/N) \tag{30}$$

$$\frac{1}{\mu(m,n)} = \cos(\pi(m-2n-1/2)/N) \tag{31}$$

Then an explicit evaluation of the matrix elements from Eq. (17) yields

$$\langle q_n | B^1_{AB} | q_{n'} \rangle = \frac{i\sqrt{2}}{2N} (1 - e^{i\pi(n-1/2)}) \cdot \begin{cases} \nu(n,n'), & 0 \leqslant n \leqslant N/4 - 1 \\ e^{i\pi(m+1/2)}\mu(n,n'), & N/4 \leqslant n \leqslant N/2 - 1 \\ \mu(n,n'), & N/2 \leqslant n \leqslant 3N/4 - 1 \\ e^{i\pi(m+1/2)}\nu(n,n'), & 3N/4 \leqslant n \leqslant N-1 \end{cases} \tag{32}$$

The classical R symmetry $(p \to 1-p,\ q \to 1-q)$ is quantally implemented by the operator whose matrix elements in the position representation are given by

$$\langle q_n | R_N | q_{n'} \rangle = \delta(n + n' + 1 - N) \tag{33}$$

$R^1_N = 1$, and thus the eigenvalues of this parity operator are ± 1. Its commutation with B^1_{AB} requires that

$$\langle q_{N-n-1} | B^1_{AB} | q_{N-n'-1} \rangle = \langle q_n | B^1_{AB} | q_{n'} \rangle \tag{34}$$

which is verified by a straightforward computation, using Eqs. (32). Thus the symmetry of reflection about the center of the square is preserved by the quantum map

$$[B^1_{AB}, R_N] = 0 \tag{35}$$

The classical symmetry of reflection about the center of each cell can also be implemented quantally. As we noted earlier, this symmetry can be thought of as a composition of T_N and R_N, and thus is not an independent symmetry; rather, it is the only canonical symmetry that is present in the map M^2_{AB} and its quantal equivalent, the matrix operator B^2_{AB}. We will briefly discuss the corresponding quantal symmetry, as it is more transparent to do each verification separately.

The required symmetry operator, in the position representation, must be given, up to a phase factor, by $\delta(n+n'+1-N/2)$ if $n' < N/2$ and by $\delta(n+n'+1-3N/2)$ if $n' \geqslant N/2$. We fix the phases by requiring that in the *momentum* representation the symmetry operator be $\delta(m+m'+1-N)$, again, up to a possible phase factor. The operator consistent with the above requirements is given in the position representation by

$$\langle q_n | R'_N | q_{n'} \rangle = \begin{cases} \delta(n+n'+1-N/2), & 0 \leqslant n' \leqslant N/2-1 \\ -\delta(n+n'+1-3N/2), & N/2 \leqslant n' \leqslant 3N/2-1 \end{cases} \tag{36}$$

The classical composition is given quantum mechanically as

$$R'_N = T_N R_N \tag{37}$$

Our choice of the overall sign of R'_N is consistent with this ordering of the operators T_N and R_N. The commutation of B^1_{AB} with R'_N is then immediate. We also note that T_N and R_N anticommute,

$$R_N T_N = -T_N R_N \tag{38}$$

We can write all the symmetry operations of the propagator B^1_{AB} as the group g, where

$$g = (I_N, -I_N, R_N, -R_N, T_N, -T_N, R_N T_N, T_N R_N) \tag{39}$$

This group is isomorphic to the point group C_{4v}, the symmetry group of a square. There are five classes, and hence five irreducible representations

of g, four one-dimensional ones and one two-dimensional representation. The four one-dimensional representations are ruled out because R and T anticommute, and hence cannot share eigenvectors from the same ray. Therefore, the eigenvectors of B^1_{AB} must be *exactly* doubly degenerate. The global symmetries of reflection about the center of the square and translation by 1/2 were *both* needed to produce this degeneracy.

In the presence of translation symmetry alone, the levels would have been nearly degenerate, displaying tunneling splitting. These would then be the simplest models exhibiting such splitting in the presence of classical chaos. For example, if we had (2/3, 1/3) bakers defined in cells A and B, we would have translation symmetry, but no reflection symmetry. If we denote the vertical left and right halves of the square matrix $G_{2N/3}$ by $G^L_{2N/3}$ and $G^R_{2N/3}$ (with dimensions $2N/3 \times N/3$) and the vertical left and right halves of the square matrix $G_{N/3}$ by $G^L_{N/3}$ and $G^R_{N/3}$ (with dimensions $N/3 \times N/6$), we have for the propagator in the position representation

$$B^3_{AB} = G_N^{-1} \begin{pmatrix} G^L_{2N/3} & 0 & G^R_{2N/3} & 0 \\ 0 & G^L_{N/3} & 0 & G^R_{N/3} \end{pmatrix} \tag{40}$$

The above model displays tunneling splitting. The level splittings due to symmetrical structures in classical phase space have been called dynamical tunneling splittings.[19] The usual tunneling splitting is due to a potential barrier, while dynamical tunneling is due to the structure of classical phase space. This has been studied in the Henon–Heiles system[19] and the anharmonic quartic oscillator.[10] The splittings are usually observed as being due to classically stable and symmetric orbits. The splittings may be irregular if the stable regions are surrounded by chaotic orbits. In the case of two noninteracting baker's maps in two cells, the splittings are solely due to classically chaotic and symmetrical structures. Let θ_i be the eigenangles of B^3_{AB} arranged in increasing order and in units of 2π. Let $\Delta_i = N(\theta_{i+1} - \theta_i)$, $i = 1, 3, 5, \ldots, N-1$. Δ_i are the tunneling splittings scaled by the factor N. Figure 3 shows Δ_i for the case $N = 150$. The splittings are seen to be highly irregular and some of them are as high as the order of Planck's constant, in contrast to tunneling splittings due to potential barriers, which are exponentially small in Planck's constant. Such high splittings may seem to complicate the prior-to-splitting ordering of the levels. We must, however, note that there is no parameter that is switched on to activate the splittings. The splittings are intrinsic and would disappear only in he classical limit. This limit is, however, reached not with a continuous parameter, but with a discrete parameter (N), and therefore we cannot tell when the ordering changed.

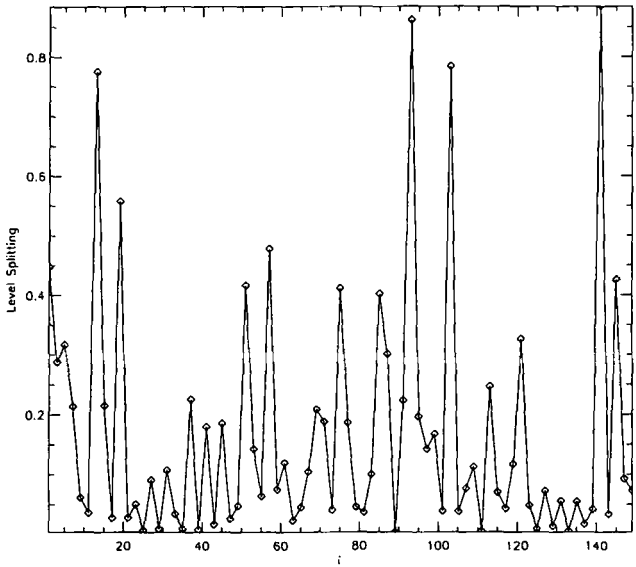

Fig. 3. The tunneling splitting Δ_i for the model B^3_{AB} with $N = 150$.

We now turn to the symmetries of the propagator B^2_{AB}, which describes a baker in cell A and a reflected baker in cell B. The propagator in the position representation is given by the matrix in Eq. (22). The explicit matrix elements can be obtained by a straightforward evaluation of geometric sums, and is given by

$$\langle q_n | B^2_{AB} | q_{n'} \rangle = \frac{i\sqrt{2}}{2N}(1 - e^{i\pi(m-1/2)}) \cdot \begin{cases} \mu(n, n'), & 0 \leqslant n' \leqslant N/4 - 1 \\ e^{i\pi(m+1/2)}\nu(n, n'), & N/4 \leqslant n' \leqslant 3N/4 - 1 \\ -\mu(n, n'), & 3N/4 \leqslant n' \leqslant N - 1 \end{cases} \tag{41}$$

where $\mu(n, n')$ and $\nu(n, n')$ are defined in Eqs. (30) and (31).

We saw above that the symmetry of reflection about the center of each individual cell is represented by the operator R'_N. A direct computation demonstrates that

$$[B^2_{AB}, R'_N] = 0 \tag{42}$$

Thus this symmetry is quantally preserved. The spatial reflection about the line $q = 1/2$ is an anticanonical symmetry, and is incorporated quantally as

an antiunitary operator. Let $|\psi\rangle$ be a vector and its reflected partner be $S_N|\psi\rangle$; then in the position representation we should have

$$\langle q_n| S_N |\psi\rangle = \langle q_n | R_N |\psi\rangle^* \tag{43}$$

Complex conjugation can be thought of as ensuring the "wrong" sign of the momentum that makes the symmetry an anticanonical one. Thus the spatial reflection symmetry is implemented by $R_N K$, where K is the conjugation operator. Spatial reflection symmetry would then require the operator to satisfy the condition

$$R_N B^{2*}_{AB} R_N = B^2_{AB} \tag{44}$$

which is once more easily verified using Eq. (41). The propagator B^2_{AB}, being unitary, has its eigenvalues located on the unit circle. This symmetry implies that they fall into two classes each of which is the complex conjugate of the other. Thus the reflection of the baker in cell B has a drastic effect on the degeneracies of the "free" propagator spectrum. It not only lifts such a degeneracy, but also "spreads" the eigenangles on the unit circle. This is one of the reasons we have introduced the second map, which, though classically of the same type as that discussed by Elskens and Kapral,[1] is nevertheless quantally significantly different. Further on we show *per se* how this may affect transport, for we are not so much interested in symmetries as in the implications they have on quantum relaxation to an equilibrium.

The complete quantum maps are given by Eqs. (25) and (26) and they include the interaction due to the overlapping baker in C. Since this map B_C given by the propagator of Eq. (24) preserves R symmetry, the complete propagator U^1_α also preserves R symmetry. The symmetries of translation and reflection about the individual cells for the "free" propagator B^1_{AB} are broken. This lifts the degeneracy of the free propagator. But the persistence of the global R symmetry implies the existence of extended eigenstates. *If the interaction is small, we can expect that the near degeneracies introduce low-frequency, large-amplitude oscillations in the relaxation process, and that the extended eigenstates contribute to large transport.* The complete propagator U^2_α, has no global or local symmetries and has no near degeneracies. This contrasts with the first case, and its implications for quantal transport are studied in the next section.

It must be noted that the usual baker's map has a time-reversal symmetry. It means that a time-reversed partner exists reflected about the secondary diagonal of the square. Such a time-reversal symmetry (which is

a combination of a phase space operation and reversing time) leads to the quantum baker's map possessing an antiunitary symmetry. We have not been able to verify the existence of the corresponding symmetry in the quantal free propagators B^1_{AB} and B^2_{AB}. It is a weak symmetry, but not a complete one. This, however, does not affect spectral features such as degeneracies or extent of eigenstates. The propagator B_{sc} [Eq. (23)] would exactly preserve time-reversal symmetry, but we take the free propagator to be B^1_{AB} because this associates one Hilbert space to the entire torus.

3.3. Further Generalizations and Models

The models we have studied above can be generalized in many ways. The individual baker's maps can be generalized to have cuts that partition the phase cells into unequal parts. One such free propagator was written above, the model B^3_{AB}. Another possible and more interesting generalization is to include more cells. The quantization of three baker's maps placed side by side and not interacting can be quantized by methods similar to that used for the propagator B^1_{AB}. The interactions can then be added in the above manner. Thus we have a vast collection of simple models with, in principle, known classical relaxation laws and quantizations. The case when there is an infinite number of cells placed along the q direction with baker's maps defined on them and the interaction is provided by *shifting* the original array by one-half in the q direction was studied as the "multi-baker map" in ref. 20, classically. The truncation with a finite number of cells (finite multibaker map) with periodic boundary conditions can then be quantized using the methods presented in this paper.

We will give some details on this last possible generalization, *primarily because the interaction does not require piecewise quantization.* As we noted earlier, the interaction B_C was associated with three independent Hilbert spaces. We will once more consider the case when the free propagator is B^1_{AB} or B^2_{AB}. The corresponding classical situation is one in which there are two noninteracting bakers in cells A and B, and the case when there is a baker's map in cell A and a reflected baker's map in cell B. Again we will consider periodic boundary conditions so that the free map is defined on a torus.

The interaction can be prepared in many ways. Consider the following case. Once more we define two baker's maps in the two cells A and B. The classical map is described by M^1_{AB} [Eq. (5)] and the quantized version is B^1_{AB} [Eq. (17)]. We then *shift* the entire map by β with respect to the original cells to the left in the q direction. This we take as the interaction. Note that if we do not shift at all ($\beta = 0$), there is no interaction; there is no mixing among the cells A and B. If we shift by 1/2, there is again no

interaction between the cells A and B. The quantization of such an interaction is straightforward and is given by

$$V^{N\beta} B^1_{AB} V^{-N\beta} \tag{45}$$

where V, defined by Eq. (15), is the position shift operator. V is diagonal in the *momentum* basis and is given by

$$\langle p_{m'} | V | p_m \rangle = e^{2\pi i(m+1/2)/N} \delta_{mm'} \tag{46}$$

The complete models with the free propagators and the interactions can be written as

$$U^3_\beta = V^{N\beta} B^1_{AB} V^{-N\beta} B^1_{AB} \tag{47}$$

and

$$U^4_\beta = V^{N\beta} B^1_{AB} V^{-N\beta} B^2_{AB} \tag{48}$$

In Eqs. (47) ad (48) the superscripts on B_{AB} and U_β are *not* powers; they are labels. The superscripts on V are, however, powers. In Eq. (48) we have used the two *different* matrix operators B^1_{AB} and B^2_{AB} to define the new operator U^4_{AB}. The classical maps are once more isomorphic to stochastic Markov chains, and their relaxation laws can be worked out. We simply state without proof that the relaxation law for the map with $\beta = 1/8$ is $C_{1/2}$, and the relaxation law for the map with $\beta = 1/16$ is $C_{1/4}$. Here $C_{1/2}$ and $C_{1/4}$ are given by Eqs. (11) and (12). The model U^3_β has translation symmetry by 1/2, while U^4_β does not. The spectrum of U^3_β is exactly doubly degenerate, while the spectrum of U^4_β is free from degeneracies.

We prove the double degeneracy of the operator U^3_β, as it does not follow from any manifest symmetry group (there is no reflection symmetry about any point, although the free propagator as well as the interaction have such symmetries). The important identity we note is the following:

$$R_N V R_N = V^{-1} \tag{49}$$

Thus we have

$$U^3_\beta = V^{N\beta} B^1_{AB} R_N V^{N\beta} R_N B^1_{AB} = (V^{N\beta} R_N B^1_{AB})^2 \tag{50}$$

due to the communication of B^1_{AB} with R_N [Eq. (35)]. The operator U^3_β can thus be expressed as the square of a simpler operator $B_0 \equiv V^{N\beta} R_N B^1_{AB}$. The operator B_0 does not commute with translations or reflections, but it

anticommutes with translations by 1/2. Thus, making use of Eq. (38), we get

$$B_0 T_N = -T_N B_0 \tag{51}$$

From this it follows that if λ is an eigenvalue of B_0, so is $-\lambda$. Thus the spectrum of $U_\beta^3 \equiv B_0^2$ is doubly degenerate.

4. QUANTUM RELAXACTION, NUMERICAL RESULTS

The quantal equivalent of the classical correlation $C_\alpha(t)$ of Eqs. (11)–(13) is the probability of transition from cell A to cell B as a function of time. Thus we consider the quantity

$$C_\alpha^Q(t) = \frac{1}{N} \text{Trace}(U^t P_A U^{\dagger t} P_B) = \frac{1}{N} \sum_{n'=N/2}^{N-1} \sum_{n=0}^{N/2-1} |\langle q_{n'}| \, |U^t| q_n\rangle|^2 \tag{52}$$

Here we may take for the unitary operator U any one of the propagators $U_\alpha^{1,2}$ or $U_\beta^{3,4}$. The P_A and P_B are projectors of the cells A and B, which in the position representation would have the form

$$P_A = \begin{pmatrix} I_{N/2} & 0 \\ 0 & 0 \end{pmatrix}, \qquad P_B = \begin{pmatrix} 0 & 0 \\ 0 & I_{N/2} \end{pmatrix} \tag{53}$$

For short times we expect $C_\alpha^Q(t)$ to be close to $C_\alpha(t)$, the classical correlation, since initial quantal phase space densities (constructed of some coherent states) propagate as if they were classical phase space densities evolving according to Liouville's equation. In this section we probe the longtime behavior using the quantal models of the three-interacting-baker's map.

We write the eigenvalue problem of the unitary operator U as

$$U|\varepsilon_j\rangle = e^{i\varepsilon_j} |\varepsilon_j\rangle \tag{54}$$

where the eigenstates are $|\varepsilon_j\rangle$ and the eigenangles are ε_j, $j = 0, 1, 2, \ldots, N-1$. We have then the time-independent part of the quantum correlation to be

$$\bar{C}_\alpha^Q = \frac{1}{N} \sum_{n'=N/2}^{N-1} \sum_{n=0}^{N/2-1} \sum_{j=0}^{N-1} |\langle q_{n'} | \varepsilon_j\rangle|^2 \, |\langle q_n | \varepsilon_j\rangle|^2 \tag{55}$$

$\bar{C}_\alpha^Q$ is also approximately the time average of $C_\alpha^Q(t)$, $\langle C_\alpha^Q \rangle$, over times longer than the inverse of the smallest eigenangle spacing. The time-averaged correlation is thus directly dependent on the distribution of the

eigenstates over the state space. If we assume that they are spread out equally in either regions A and B, we would get $\bar{C}_\alpha^Q$ to be approximately equal to 1/4, which is the classical time average. Deviations from this must then have essentially a quantal origin.

In Figs. 4–7 we show the transition probability $C_\alpha^Q(t)$ for various values of α and N. In all the figures the solid line represents the quantum model with global R symmetry (labeled Quantum 1), U_α^1, while the dotted line represents relaxation in the quantum model U_α^2 (labeled Quantum 2) which has no global symmetries. Figure 4 shows the case of $\alpha = 1/8$, in the propagators. The dashed curves shown in all the figures are the classical relaxation curves of Eqs. (11)–(13) for both models. The short-time behaviors of the same models is shown in Fig. 7 for emphasis. Recollect that N is the inverse of Planck's constant, so that we have probed models in a broad range from strongly quantal to largely semiclassical.

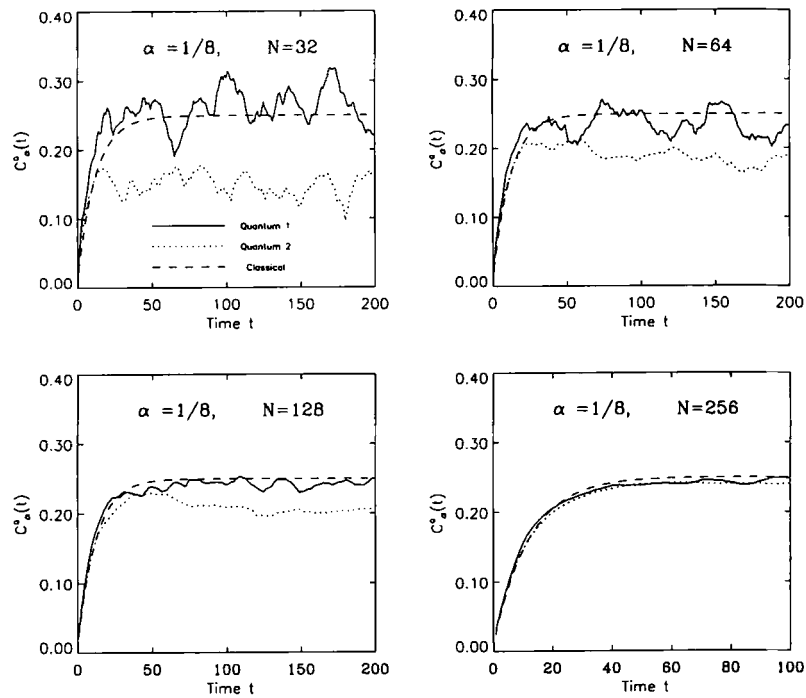

Fig. 4. The rate of transition from cell A to cell B. The initial distribution is uniform over cell A. The solid lines are for the quantum model F_α^1, indicated in this and subsequent figures as Quantum 1. The dotted lines are for the quantum model F_α^2 (Quantum 2). All the dashed lines are the classical correlations given by Eqs. (11)–(13). Shown here are different values of inverse Planck's constant, N, for the case $\alpha = 1/8$.

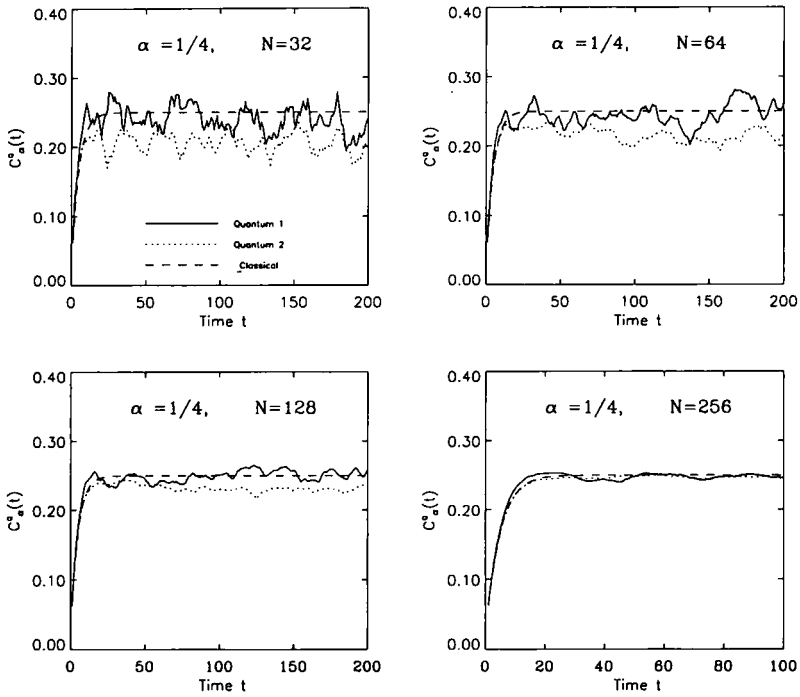

Fig. 5. Same as Fig. 4, except the value of $\alpha = 1/4$.

Several features are at once apparent. The quantal transport for both models $U^{1,2}_{\alpha}$ is slightly higher than the classical transport for short times (Fig. 7) and this difference decreases with decreasing Planck's constant. We attribute this to quantal tunneling between the cells A and B. Note that if we had used the block diagonal matrix B_{sc}, Eq. (23), as our free propagator for U^{1}_{α}, the classical and quantal transport would match *exactly* for the first time step. The tunneling effects are quite small, and in part justify our neglecting them during the interaction time step.

Apart from tunneling effects, we see that quantal transport due to the propagator U^{2}_{α}, the model with no global symmetry, follows the classical relaxation curve very closely much beyond the linear regimes. The quantal relaxation curve follows the classical one, up to a time when quantal effects manifest themselves as saturation of transport, with an average significantly lower than the classical saturation value of 1/4. There are fluctuations about this average that become smaller when Planck's constant is decreased. As we noted earlier, lower average is implied if the eigenstates

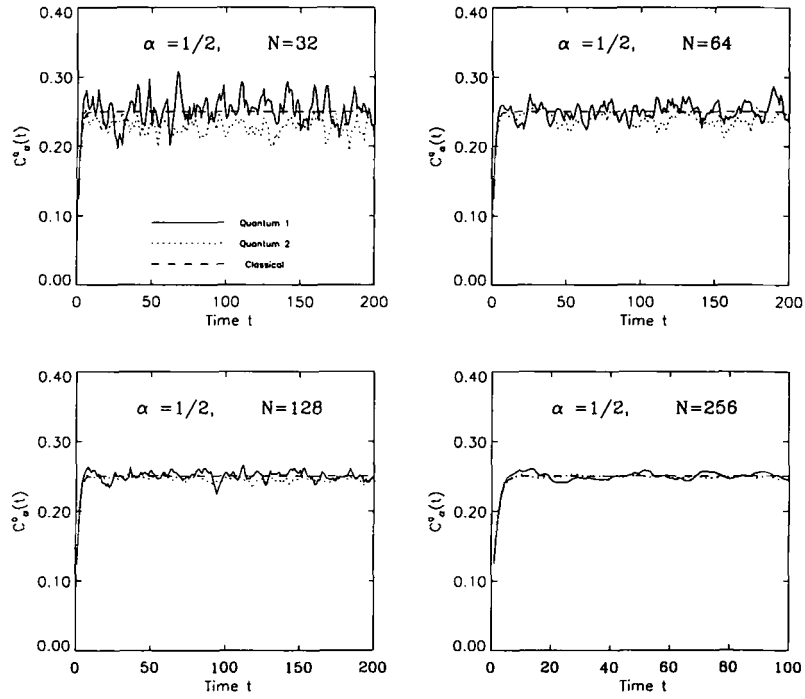

Fig. 6. Same as Fig. 4, except the value of α is 1/2.

are not spread between the cells equally. *Thus we are led to the appearance of "localized" eigenstates.* For increasing N, or decreasing Planck's constant, the saturation occurs at a higher value, tending toward the classical uniform distribution.

Figures 5 and 6 show the classical and quantal relaxation curves for the parameters $\alpha = 1/4$, 1/2. On increasing the "interaction strength" α the average quantal steady state approaches the classical one, and is implied by a gradual delocalization of the eigenstates. Such effects have been observed in the quantized standard map, and we will discuss this below. The same figures discussed above also show the relaxation behavior of the quantum map U_α^1, corresponding to the classical map F_α^1. As noted earlier, the map F_α^1 has the same relaxation laws as F_α^2, but we observe that the quantal relaxation behavior of the corresponding map U_α^1 is vastly different from that of U_α^2; there is an anomalously large transport and large fluctuations about the *classical* average. This is especially apparent for smaller values of Planck's constant, that is, when the quantum effects are fully operative. The

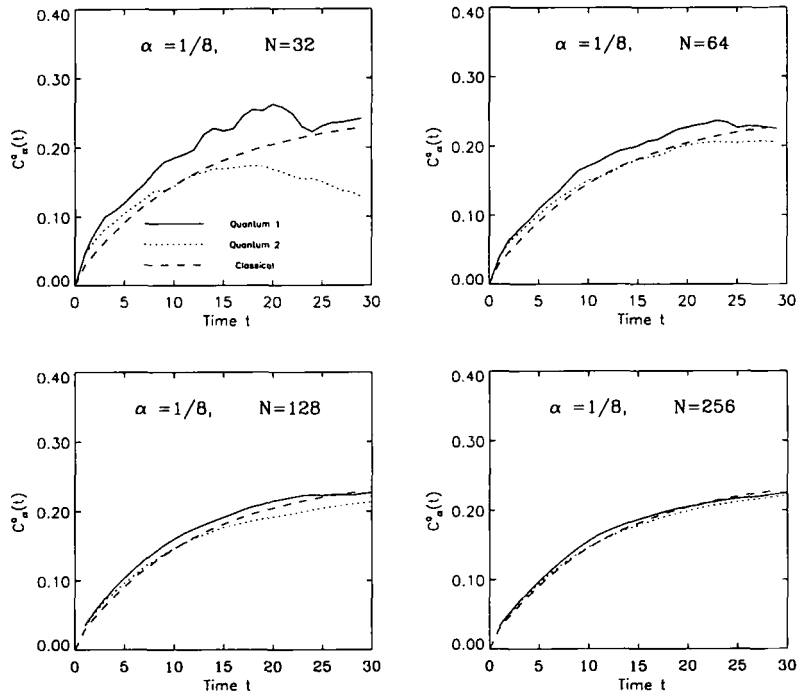

Fig. 7. Same as Fig. 4, but shown are the correlations over a shorter time scale to emphasize short-time features.

resonant transport between cells A and B actually *decrease* with Planck's constant until the average becomes slightly lower than the classical equilibrium, indicating a weak localization. This is apparent, for example, in Fig. 4 for $N=64$.

In Fig. 8 we plot the relaxation in the models $U_{1/8}^{3,4}$ and $U_{1/16}^{3,4}$ for $N=64$. We note that the model U_β^3 (Quantum 3 in the figures), with exactly degenerate spectrum, has very large fluctuations about the equilibrium, while the model U_β^4 (Quantum 4 in the figures) has small fluctuations and is similar in behavior to the model U_α^2, which for comparison we plot in the same figures. The larger fluctuations in the case of the degenerate model U_β^3 is due to the lack of phase cancellations, as there are only $N/2$ different eigenangles.

Recall that the map U_α^1 has the global symmetry of reflection about the center of the square R. The commutation of R_N with U_α^1 implies that the eigenstates are of either even or odd parity; there are no other sym-

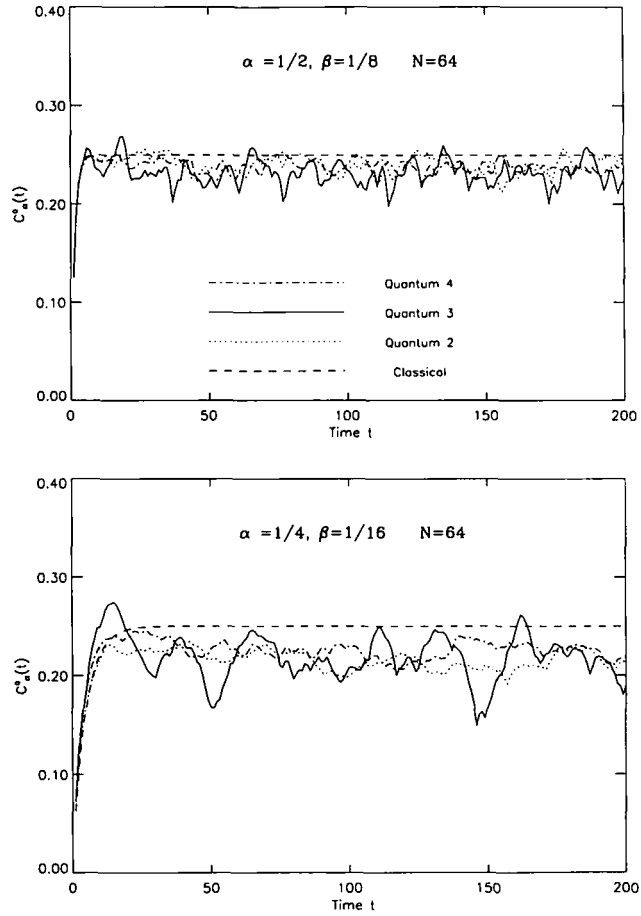

Fig. 8. Correlations of the models $U_\beta^{3,4}$ (Quantum 3 and 4) compared with the classical relaxation and the relaxation of the model U_α^2.

metries, the translation symmetry of the free propagator B^1_{AB} being broken by the interaction. Any eigenstate can be written as

$$\begin{pmatrix} |\psi\rangle \\ \pm R_{N/2}\,|\psi\rangle \end{pmatrix} \tag{56}$$

and is hence delocalized, in the sense that they are distributed exactly equally (in the position basis) over states that span cells A and B. This would in part lead to the higher averages. The short-time behavior of the

model $U^1_{1/8}$, (Fig. 7) shows significantly higher transport rate than the classical. Although the results shown here are all for the cases when N is a power of 2, unpublished results indicate that there are no surprises for other values of N. The relaxation behavior qualitatively follows those cases illustrated here.

We show several eigenstates in Fig. 9. Four eigenstates of $U^2_{1/8}$ for

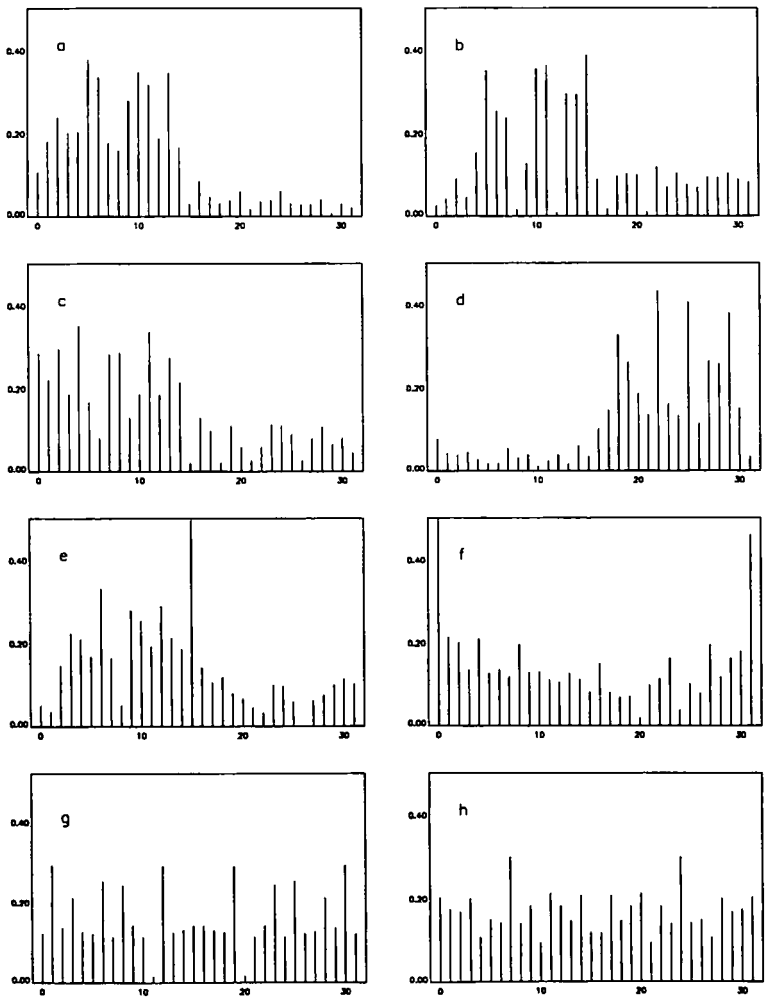

Fig. 9. (a–f) Eigenfunctions of the quantum map 1, $U^1_{1/8}$ for $N = 32$. (a–e) Eigenfunctions largely localized to either cell A or cell B; (f) a largely delocalized eigenfunction. (g, h) Two eigenfunctions for the quantum map 2, $U^2_{1/8}$. The global R symmetry is evident.

$N = 32$ are shown in Figs. 9a–9f. The localization of some eigenfunctions to either cell A $(n \leqslant N/2 - 1)$ or cell B $(n \geqslant N/2)$ strongly suggests that the localization is due to the lack of classical diffusion. The R symmetry of each individual cell is broken by the interaction, but may be weakly present. Not *all* the eigenstates are thus localized; a significant number of them are largely delocalized and an example is shown in Fig. 9f. This indicate that the localization we have observed is not "perturbative." Indeed we have coupled at least 1/8 of the position states by the interaction.

In this last figure the scarring from the fixed points at the corners of the square is evident. The structure of eigenfunctions within regions of localization is still under study.[5] The quantum baker's map eigenfunctions were scarred by many classical periodic orbits.[15] Periodic orbit scarring has been observed in many systems[22] since it was first observed in the stadium eigenfunctions.[16] Scarring is also a type of localization, and we can expect that the models we have studied, which are coupled bakers' maps, will display this phenomenon. In these cases the structure of eigenfunctions within the localized regions need to be random, but can be very regular. The set of periodic orbits that scar certain eigenfunctions will then be dependent on features of classical transport. Some eigenstates of $U^1_{1/8}$ are shown in Figs. 9g and 9h and the R symmetry is apparent. The plots are the moduli of the eigenstates in the position basis.

5. DISCUSSION

We have used models of three interacting baker's maps to show the influence of localization and delocalization on quantal relaxation to an equilibrium. The delocalization in the eigenstates of the map U^1_α is simply due to the global R symmetry. The localization of the eigenstates of the map U^2_α was gradually removed by increasing the parameter α, which also effects a larger classical transport. Thus the same parameters affect naturally the classical rate laws and quantal eigenstates.

Previous studies that have observed similar effects include the much-studied quantized standard map variously known as the quantum kicked rotor or the quantum Chirikov map.[5] The classical model is a kicked rotor with the time-dependent Hamiltonian

$$H = p_\theta^2/2 + k \sin\theta \sum_{n=-\infty}^{\infty} \delta(t - nT) \tag{57}$$

Above a critical value of $K = kT$, the classical motion becomes unbounded, and a diffusive growth in momentum, given by

$$\langle (p_\theta - \bar{p}_\theta)^2 \rangle = Dt \tag{58}$$

is observed. Here D is the diffusion constant $= K^2/2$. The quantal behavior of this time-dependent system was observed to exhibit classical diffusive growth in momentum for short times and then a saturation. Thus quantum mechanics is supposed to "suppress classical chaos." This reflects the localization of the eigenstates in the unperturbed ($k = 0$) basis. Although this model has been mapped on to a 1D tight-binding model of solid-state physics,[17] the dynamical origins of localization are not yet fully understood.[10]

The models we have begun to study in this paper *differ from the standard map in the two essential and related details; the motion is always bounded, and the diffusive growth is replaced by a relaxation to a unique equilibrium state via mixing*. The standard map on the torus has also been quantized[5] and it should be interesting to campare these two models. The classical dynamics of the three bakers is exactly solvable, and also the dynamics has a simple geometrical picture. The standard map on the torus, on the other hand, has more parameters, thus providing us with a range of models.

The three-baker's map models the motion on a single energy surface of a time-independent Hamiltonian system in which different chaotic regions are connected by an interaction that depends on some parameter. Classical transport in the presence of partial barriers[9] such as cantori presents such a situation. There is chaotic mixing within separate regions of phase space and a slow crossing over between these regions. In other words, a single phase point spends a long time in each region before crossing over into the next.

Recently Bohigas *et al.*[10] studied such transport with the help of random matrix theories and illustrated it with the example of an anisotropic coupled quartic oscillator. They introduced the term "semiclassical localization" as opposed to the "dynamical localization" in the standard map. The localization in the quantal three-baker's map is presumably connected to the "semiclassical localization," although there is nothing really semiclassical about it. The models introduced here may provide an ideal testing ground to further study this phenomenon, as they have no additional complications, and are finite-dimensional quantum systems requiring no artificial truncation of a basis.

5.1. Break Time and Localization

While saturation of relaxation or suppression of diffusion may be implied by localization of some eigenfunctions in a particular basis, the natural question is, why this localization at all? We dwell briefly and qualitatively on the notion of the break time[18,2] as a mechanism that

localizes eigenstates, at least in the kind of situations we have modeled using the three-bakers' maps. Classical mechanics is characterized by the continuity of phase space and the consequent possible long-time exploration of trajectories on fine scales, while in the quantum mechanics of bounded systems the energy spectrum is discrete and the evolution is quasiperiodic at best. The discreteness of the spectrum is resolved after a finite time, the break time, which is roughly proportional to the average level density, in this case, eigenangle density [we have defined the eigenangles as in Eq. (54)]. Eigenfunctions can be found as the time Fourier transform of propagating an initial state, and the effective exploration of the state occurs within the break time. Thus the eigenfunctions will be localized if the exploration (in our case simply in the configuration space) is limited. For instance, in the three-baker's models, states localized well away from the line $q = 1/2$ have such a possibility of becoming localized, leading to a localized eigenstate.

6. SUMMARY

We have discussed several models showing simple relaxation to an equilibrium state, both classically and quantum mechanically. In the absence of global symmetries, the relaxation can be significantly retarded, and even suppressed by quantum effects. In these cases we find significant localization of the eigenstates. Even in the presence of global symmetry and in the deep semiclassical regime we find a small difference between in the quantum steady state and the classical steady state, implying the existence of weak localization. These simple models of quantal transport in bounded systems thus display a rich structure. We have also introduced some simple models of tunneling between classically disjoint and chaotic regions of phase space.

APPENDIX A

Elskens and Kapral[1] showed that the three-bakers' transformation is isomorphic to a finite Markov shift for rational values of α. We include the partitions for completeness, and to demonstrate that the maps $F_\alpha^{1,2}$, have identical partitions and hence identical relaxation laws given by Eqs. (11)–(13). The details differ from those of ref. 1 in notations and scale, and also in the interchange of position and momentum coordinates. The latter change means that our forward-iterated partitions are the backward-iterated partitions of ref. 1 and vice versa.

If $\alpha = a/b$ for a and b integers, one partitions the unit square of the phase space into $2b$ vertical bands consisting of rectangles $[k/2b,$

$(k+1)/2b) \times [0, 1)$; k is an integer such that $0 \leqslant k \leqslant 2b-1$. For $b=2$, this partition is illustrated in Fig. 2(a). The rectangles of the partition Q_k (also called "atoms") are labeled by integers. The forward iterate of this partition of the phase space square is shown in Fig. 2b for the map $F^1_{1/2}$ and in Fig. 2c for the map $F^2_{1/2}$. These maps were defined in the text by Eqs. (1)–(7).

The stable and unstable directions of both maps are globally parallel to the p and q axes respectively, just as for the individual bakers' map. A forward iterate of the partition sits within the original partition in such a way that there is no further partitioning in the stable direction, but there are additional partitions in the unstable direction. In other words, the unstable manifolds that form part of the partition in Fig. 2a are a proper subset of the unstable manifolds that form part of the partition in Fig. 2b. Similar conditions are satisfied by the part of the partition boundary that is formed by stable manifolds, under backward iterations.

The forward partitions are labeled by symbols whose first integer represent the atom they belong to at "present" and the second integer refers to the atom they just came from. Thus the phase square gets partitioned horizontally by forward iterates into finer regions. The backward iterates, not illustrated here, similarly partition phase space vertically. This is the requirement for a partition to be a Markov partition.[11]

We see from comparing Figs. 2b and 2c that the partition works for both the maps $F^{1,2}_{\alpha}$ in an essentially identical way. A measure, or probability, equal to their area is assigned to the atoms, $p_k = \mu(Q_k)$, and we write also $p_{kl} = \mu(Q_{kl})$. The transition probability from atom Q_l to atom Q_k is $m_{kl} = \mu(Q_{kl})/\mu(Q_l) = 2b\mu(Q_{kl})$.

The matrix of transition probabilities for $\alpha = 1/2$, obtained from either Fig. 2b or Fig. 2c, is then

$$\begin{pmatrix} 1/2 & 1/4 & 1/4 & 0 \\ 1/2 & 1/4 & 1/4 & 0 \\ 0 & 1/4 & 1/4 & 1/2 \\ 0 & 1/4 & 1/4 & 1/2 \end{pmatrix} \tag{A1}$$

The case of $\alpha = 1/2$ is also isomorphic to a finite Bernoulli shift, as shown in ref. 1. The Markov matrices corresponding to $\alpha = 1/4$ and $1/8$ may be similarly constructed. These are all double stochastic matrices; because the atoms of the partition had equal measures, they have an unique equilibrium state corresponding to the uniform distribution.

The correlation function in the text may now be evaluated. The densities we have chosen are particularly simple, as they can be constructed

out of the atoms of the Markov partition. Then the evaluation of correlations is equivalent to the problem of finding the powers of the Markov matrices. This leads to Eqs. (11)–(13).

APPENDIX B

Here we give some details of the quantization of M^1_{AB}, which is simply two bakers sitting side by side. Since, naturally, this depends strongly on the quantization of a lone baker. We refer to refs. 3, 7, and 15 for elaborations and emphasize here the differences that arise. The lone baker map *on the unit square* is given by the transform

$$(q', p') = \begin{cases} (2q, p/2), & 0 \leqslant q < 1/2 \\ (2q-1, (p+1)/2), & 1/2 \leqslant q < 1 \end{cases} \tag{B1}$$

Its quantization proceeds by mimicking quantally the classical partition into left and right vertical rectangles (Fig. (1a), with a partitioning of the Hilbert space into two orthogonal subspaces of dimensions $N/2$, represented by L^Q and R^Q. If $|\phi^L\rangle$ is a vector in L^Q and $|\phi^R\rangle$ is a vector in R^Q, these spaces are specified by requiring

$$\langle q_n \mid \phi^L \rangle = 0 \qquad \text{if} \quad n \geqslant N/2 \tag{B2}$$

$$\langle q_n \mid \phi^R \rangle = 0 \qquad \text{if} \quad n \leqslant N/2 - 1 \tag{B3}$$

Thus we require N to be even. Classically the left partition is stretched in the q direction and contracted in the p direction, so that it forms the horizontal bottom half of the phase square. The right vertical partition is similarly transformed into the upper horizontal half of the phase square (Fig. 1b). Thus the vector space is also likewise divided into the orthogonal subspaces spanned by the vectors ψ^B and ψ^T specified by the following conditions:

$$\langle p_m \mid \psi^B \rangle = 0 \qquad \text{if} \quad m \geqslant N/2 \tag{B4}$$

$$\langle p_m \mid \psi^T \rangle = 0 \qquad \text{if} \quad m \leqslant N/2 - 1 \tag{B5}$$

This dynamics is quantally translated by requiring that each vector from the subspace spanned by $|\phi^L\rangle$ be transformed into a vector in the subspace spanned by the vectors $|\psi^B\rangle$. In the *momentum* representation the transform of an $N/2$-component vector ϕ^L from the subspace L^Q written in the position representation is given by the vector

$$G_{N/2}(\phi^L) \tag{B6}$$

See ref. 7 for the original quantization. Here $G_{N/2}$ is the $N/2 \times N/2$ Fourier transform defined for N sites by Eq. (14).

Since any vector can be written as a sum of vectors from the subspaces L^Q and R^Q, the quantal propagator in the *mixed representation* is thus given by the matrix

$$\begin{pmatrix} G_{N/2} & 0 \\ 0 & G_{N/2} \end{pmatrix} \tag{B7}$$

Transforming to the position basis, we get the quantum baker's map

$$B_N = G_N^{-1} \begin{pmatrix} G_{N/2} & 0 \\ 0 & G_{N/2} \end{pmatrix} \tag{B8}$$

In the quantum baker's transformation outlined above, the partition of phase space before and after the transformation fell naturally into subspaces that had exact quantal projectors associated with them, and could be easily writen in either the position (before the transformation) or momentum (after the transformation) basis (Figs. 1a and 1b). A similar partition before the transform is shown in Fig. 2a for the map $M^1{}_{AB}$. The partitioning of the square into four equal squares after the transformation cannot be implemented quantally. We can, however, consider the transformation of the partitions 1 and 3 together into the bottom half of the square, and similarly partitions 2 and 0 together into the top half of the square. This is the origin of tunneling when we quantize the map $M^1{}_{AB}$. We will see that this partitioning is sufficient to describe the quantum map.

We again mimick the partitioning of the classical phase space before the transformation (Fig. 2a) by dividing the Hilbert space into four orthogonal vector spaces of dimensions $N/4$ each. Thus we will require N to be a multiple of 4. Let the four orthogonal spaces have representative vectors $(\phi^3, \phi^2, \phi^1, \phi^0)$, and we will require that

$$\langle q_n \mid \phi^3 \rangle = 0 \qquad \text{if} \quad n \geq N/4 \tag{B9}$$

with similar conditions on the other vectors.

The transformation of partitions 3 and 1 to the lower horizontal half of the square is thus once more implemented quantally as a Fourier transform on $N/2$ sites. Thus we write the transformed vector in *momentum* representation as

$$G_{N/2} \begin{pmatrix} \phi^3 \\ \phi^1 \end{pmatrix} = (G^L_{N/2} \mid G^R_{N/2}) \begin{pmatrix} \phi^3 \\ \phi^1 \end{pmatrix} \tag{B10}$$

Here the vector to the right of the $G_{N/2}$ matrix is written in the *position* representation. We have split the matrix $G_{N/2}$ into a right and a left half, because these are the operators that act on the individual vectors from the subspaces 3 and 1, respectively. They are *rectangular* matrices of dimensions $N/2 \times N/4$. A similar argument holds for the transformation from 2 and 0 to the top horizontal half of the space square. Thus we get the propagator of M^1_{AB} in the mixed representation

$$\begin{pmatrix} G^L_{N/2} & 0 & G^R_{N/2} & 0 \\ 0 & G^L_{N/2} & 0 & G^R_{N/2} \end{pmatrix} \tag{B11}$$

Upon transforming to the position representation via the inverse Fourier transform, we get the propagator (17). Quantization of the other maps, such as like M^2_{AB}, follows from similar arguments.

ACKNOWLEDGMENTS

Both authors express their thanks to the National Science Foundation for their partial support. A. L. also thanks the Department of Physics, SUNY, Stony Brook, for partial financial support and Dr. J. J. M. Verbaarschot for useful discussions.

REFERENCES

1. Y. Elskens and R. Kapral, *J. Stat. Phys.* **38**:1027 (1985).
2 M. J. Giannoni, A. Voros, and J. Zinn-Justin, eds., *Chaos and Quantum Physics* (Elsevier, Amsterdam, 1990).
3. L. E. Reichl, *The Transition to Chaos in Conservative Classical Systems: Quantum Manifestations* (Springer-Verlag, New York 1992).
4. M. C. Gutzwiller, *Chaos in Classical and Quantum Mechanics* (Springer-Verlag, New York, 1990).
5. F. M. Izrailev, *Phys. Rep.* **196**:299 (1990).
6. J. H. Hannay and M. V. Berry, *Physica D* **1**:267 (1980).
7. N. L. Balazs and A. Voros, *Ann. Phys.* (N.Y.) **190**:1 (1989).
8. E. B. Bogomolny, *Nonlinearity* **5**:805 (1992).
9. R. S. MacKay, J. D. Meiss, and I. C. Percival, *Physica D* **13**:55 (1984).
10. O. Bohigas, S. Tomsovic, and D. Ullmo, preprint; *Phys. Rep.*, to appear.
11. I. P. Cornfeld, S. V. Formin, and Ya. G. Sinai, *Ergodic Theory* (Springer-Verlag, Berlin, 1982).
12. P. W. O'Connor and S. Tomsovic, *Ann. Phys.* (N.Y) **207**:218 (1991).
13. P. W. O'Connor, S. Tomsovic, and E. J. Heller, *Physica D* **55**:340 (1992).
14. A. M. O. De Almeida and M. Saraceno, *Ann. Phys.* (N. Y.) **210**:1 (1991).
15. M. Saraceno, *Ann. Phys.* (N.Y.) **199**:37 (1990).

16. S. W. McDonald and A. N. Kaufman, *Phys. Rev. Lett.* **42**:1189 (1979).
17. Shmuel Fishman, D. R. Grampel, and R. E. Prange, *Phys. Rev. Lett.* **49**:509 (1982).
18. E. J. Heller, *Phys. Rev. A* **35**:1360 (1987).
19. M. J. Davis and E. J. Heller, *J. Chem. Phys.* **75**:246 (1981).
20. P. Gaspard, *J. Stat. Phys.* **68**:673 (1992).
21. I. C. Percival, In *Chaos and Quantum Physics*, M. J. Giannoni, A. Voros, and J. Zinn-Justin, eds. (Elsevier, Amsterdam, 1990).
22. E. J. Heller, In *Chaos and Quantum Physics*, M. J. Giannoni, A. Voros, and J. Zinn-Justin, eds. (Elsevier, Amsterdam, 1990).